Holzforschung, Vol. 66, pp. 497–503, 2012 • Copyright © by Walter de Gruyter • Berlin • Boston. DOI 10.1515/HF.2011.180

Revisiting the neutral axis in wood beams

Philip M. Davis, Rakesh Gupta and Arijit Sinha*

Department of Wood Science and Engineering, Oregon State University, Corvallis, Oregon, USA

*Corresponding author.
Assistant Professor, Department of Wood Science and Engineering, Oregon State University, Corvallis, OR 97331, USA
E-mail: arijit.sinha@oregonstate.edu

Abstract

For wood beams, it is often assumed that the neutral axis (NA) is located at the centroid of the beam. This would be the case for isotropic and homogeneous materials but these prerequisites are not valid for wood. The varying grain patterns and knots located throughout wood make wood anisotropic and non-homogeneous. Knowledge of the true location of the neutral axis would facilitate a better understanding of the mechanical behavior of wood beams. To analyze this question, a digital image correlation technique (speckle photography) was applied while wood beams with the dimensions 25×25 mm^2 and 38×89 mm^2 were loaded in bending. The NA was determined by axial strain plots. From the data obtained it is was observed that the neutral axis of 25×25 mm^2 beams is located below the centroid while for 38×89 mm^2 beams NA was above the centroid. As would be expected, knots change the location of the NA depending on their location in the beam.

Keywords: digital image correlation; Douglas fir; knots; mechanical behavior; orthotropic materials.

Introduction

The neutral axis (NA) for beams is defined as a longitudinal plane in the cross section that does not experience any stress and change in length when the beam is subjected to bending. The portion of the cross section above the NA will experience tension and the portion below compression while in bending. Accordingly, the NA is the location where the stress changes from tension to compression (Bedford and Leichti 2001). If the modulus of elasticity (MOE) of the material in tension and in compression is equal, the areas of tension and compression will also be equal and the NA is in the middle of the beam (Gere and Timoshenko 1997). This is true for isotropic and homogeneous materials. For wood beams, this may not be always the case (Betts et al. 2010). Knots and various grain patterns cause additional deviations from the idealized state.

As wood is an orthotropic material, its properties are dependent on three mutually perpendicular directions (Kretschmann 2011). For a small clear specimen, tensile modulus and strength are greater than compressive modulus and strength (Kollen-Cumbie 2008), while in solid sawn lumber the reverse is true (Schniewind 1981; Kretschmann 2011). Kollen-Cumbie (2008) determined the strength and MOE of Douglas fir in bending, tension, and compression on small clear specimens (Table 1). The strength of full-size Douglas fir lumber in bending, tension and compression was analyzed by Green and Evans (1987) and differences between small and full-size specimens were observed. These differences can probably be explained by the position of the NA when calculated on the basis on the composite beam theory (Redler 2006). Theoretically, as shown in Figure 1, when $MOE_{tensile}>MOE_{compr}$, the NA is located below the centroid and in the opposite case is located above the centroid. The grain angle (GA) has also to be taken into account. The bending strength varies drastically as a function of GA, being greatest when load and GA are perpendicular to one another and lowest when the two parameters are parallel (Kollman and Cote 1968).

Comparisons of wood with reinforced concrete are conclusive with regard to the location of the NA, as the latter is also non-homogenous. Lopes and Bernardo (2004) studied the movement of the NA in high-strength concrete beams in pure bending with changing reinforcement ratios. They found that the depth of the NA moves upward as the longitudinal tensile reinforcement ratio was increased, i.e., the NA rises up away from the centroid as cracks develop in reinforced concrete and steel begins to yield. Similarly, Betts et al. (2010) tested 25×25 mm^2 Douglas fir samples in third-point bending to characterize the location of the NA by optical methods. As would be expected, in a clear wood beam the NA was below the centroidal axis (Figure 2) because in Douglas fir beams $MOE_{tensile}>MOE_{compr}$ (Kollen-Cumbie 2008). Figure 2 also shows the location of NA in the presence of knots in the tension and in the compression zone. The strong influence of this parameter is plausible and illustrated in the Figure.

Theoretical results (Redler 2006) and experimental results of Betts et al. (2010) confirm the dependence of the position of the NA on various parameters. The present study addresses this issue by determining the effects of knots and grain patterns on the NA by means of digital image correlation (DIC) (speckle photography). DIC is a full field, non-contact and established technique. Its suitability was demonstrated in the past two decades for analyzing stresses and the corresponding strains in the context of various problems, such as, characterizing wood specimen under different applications (Choi et al. 1991; Murata and Kanazawa 2007; Betts et al. 2010; Kang et al. 2011), analyzing microstructure in failure of wood (Jernkvist and Thuvander 2001; Ljungdahl et al. 2006; Modén and Berglund 2008), wood-based composites (Serrano and Enquist 2005; Jeong et al. 2010; Sebera and Muszyński 2011), and complex structural assemblies like shear-walls (Sinha and Gupta 2009).

Table 1 Average strength and modulus of elasticity values for Douglas fir in bending (19×19×292 mm), compression (25×25×100 mm), and tension [dog-bone shaped 6.4×(50–25)×230 mm] in three orthogonal directions, tested by Kollen-Cumbie (2008) according to ASTM D 143. The number of samples per test configuration and the coefficient of variation are shown in parentheses (*n*, COV).

	Bending		Tension		Compression	
Anatomical direction	Strength (MPa)	MOE (GPa)	Strength (MPa)	MOE (GPa)	Strength (MPa)	MOE (GPa)
Radial	8.763 (11, 4)	0.669 (11, 4)	5.244 (9, 7)	0.009 (9, 11)	7.73 (10, 30)	0.530 (10, 26)
Tangential	4.830 (10, 8)	0.676 (10, 4)	2.691 (10, 14)	0.010 (10, 11)	8.83 (15, 19)	0.526 (15, 18)
Longitudinal	86.25 (10, 8)	15.53 (10, 10)	75.21 (9, 10)	6.49 (9, 10)	52.51 (11, 4)	4.57 (11, 2)

MOE, modulus of elasticity.

In the present work, specifically, we examined the location of the NA in beams 25×25 mm^2 of both Douglas fir and other wood species, and for beams 38×89 mm^2 of Douglas fir, and also estimated qualitatively the influence of knots on the NA.

Materials and methods

Sample preparation

Beams from clear wood (25×25×406 mm^3) of Douglas fir, Southern yellow pine, Hem fir, alder, and oak were prepared (Table 2, Figure 3a). In addition, a beam (25×25×406 mm^3) of Hem fir was tested with a knot in compression and then (after inversion) in tension. Four larger Douglas-fir samples (38×89×1000 mm^3) were also tested (Table 3, Figure 3b). Sample 1 was a clear specimen, Sample 2 contained a knot in compression, Sample 3 contained a knot in the center, and Sample 4 contained a knot in tension. A quadratic hollow steel beam, 25×50 mm^2 with 1.65 mm wall thickness, was also tested (loaded to only about 6.0 kN) for validation of the data-acquisition system and to allow comparison of results from the wooden beams with those from a homogeneous specimen.

Digital image correlation

The test beams were sprayed with a coat of white paint and then overlaid with a black speckle pattern (Figure 4a). The setup consisted of a pair of cameras (placed on tripods) arranged at an angle between 30° and 60° to take stereoscopic images of the area of interest (Figure 4b). For more details on DIC please see Sutton et al. (1983) and Sinha and Gupta (2009). The time between images taken under load (0.05 s) was set to be short enough for the software to recognize the speckle pattern, but long enough to avoid the collection of more images than needed. The images were analyzed by the VIC-3D software (Correlated Solutions Inc., Columbia, SC, 2005). It is necessary to calibrate the system before making quantitative measurements.

Testing

The 25×25 mm^2 beams were loaded with a single load point at the middle of the 356 mm span (ASTM D143) at a rate of 5 mm min^{-1} with the cameras capturing images every 0.05 s. The nominal 38×89 mm^2 beams were loaded with two load points spaced 356 mm apart and centered in a 965 mm span (similar to ASTM D198) at a rate of 5 mm min^{-1} with a maximum load set at 10 kN. The cameras captured images every 5 s. The larger beams were not loaded to failure because the intention was to turn each beam by 180° and load it again to obtain more results. These beams were rotated, keeping the front face of the beam facing the camera view. The loading and image capture rates were adapted to the VIC-3D software capacity. All 25×25 mm^2 specimens were loaded to failure except the specimen with a knot. That specimen was first loaded with the knot in tension and was not loaded to failure; after inverting the beam, however, the specimen was loaded to failure. All beams were supported on a pin support (allowed rotation but no translation in any

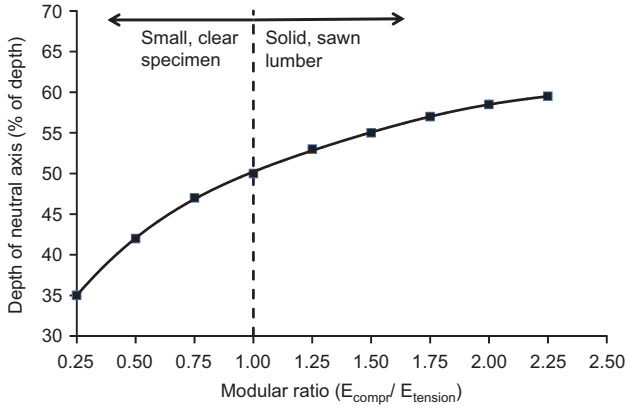

Figure 1 Depth of neutral axis vs. modular ratio according to classical beam theory (compiled from Redler 2006).

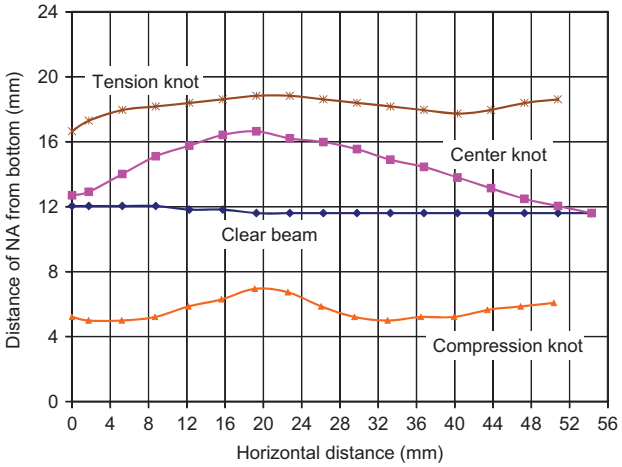

Figure 2 Neutral axis location for 25×25 mm Douglas fir sample (created with data from Betts et al. 2010).

Table 2 Distance of the neutral axis (NA) from the bottom (from the tension face) for clear 25×25 mm^2 beams.

Specimen no.	Species *Scientific name*	Distance of NA (mm)
1	Douglas fir *Pseudotsuga menziesii*	11.68
4	Southern yellow pine *Pinus palustris*	11.68
5	Hem fir *Tsuga heterophylla*	10.16
6	Alder *Alnus rubra*	11.18
7	Oak *Quercus rubra*	11.43
	Average	11.22

Specimens 2 and 3 with knot, therefore not listed.

direction) at one end and on a roller support (allowed translation along the longitudinal axis of the beam but no translation perpendicular to it and no rotation) at the other end. The load head was rounded as usual.

Image data processing

Image data processing was carried out with VIC 3D software: after data collection an area of interest (AOI) was defined for analysis (Figure 4a). The AOI should be adapted to the computing capacity of the program. A contour plot of the axial strain permits the determination of the NA location (Figure 5).

Results and discussion

25×25 mm^2 beams

Axial strain (ε_{xx}) contour plots were produced for each specimen and the plot at the maximum load was the basis for approximating the location of the NA because the NA is most clearly defined here. The location of NA is not a clear straight line but a jagged one, and its location is varies along the beam. An averaging process is needed to ascertain the NA (Figure 6b, Table 2).

Despite statistical variations, all NAs of the various species are consistently located below the centroid of the beam. The range of locations varies from 1 mm to 2.5 mm below the centroid (half-way distance) of the beam. For comparison, Betts et al. (2010) as a reference paper for small clear specimens, found the NA to be approximately 1.1 mm below the centroid of the beam. The variation between the species is probably attributable to their different values for tensile and compressive modulus of elasticity.

With a knot in the tension zone, the NA shifted upward and was found to be 3 mm above the centroid of the Hem fir beams. With a knot as weak point in compression, the NA shifted expectedly down and was approximately 2.5 mm

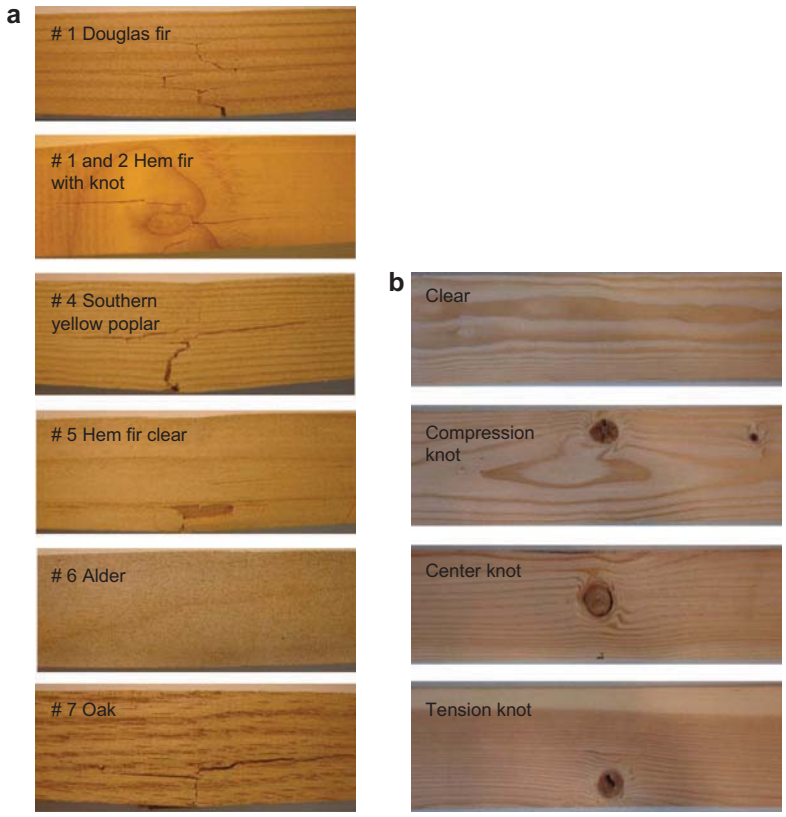

Figure 3 Examples for the wood specimens tested, of dimension (a) 25×25 mm^2 and (b) 38×89 mm^2.

Table 3 Neutral axis (NA) locations from the bottom (from the tension face), and deviation from centroid of Douglas fir beams 38×89 mm^2.

Specimen	Dimensions of beam		Distances (mm)		
	Length (mm)	Cross-cut (mm)	Half-distance	NA from bottom	Δ Deviation NA[a]
1a (clear)	1619.3	38×89.4	44.7	46.2	+1.5
1b (inverted, clear)	1619.3	38×89.4	44.7	47.1	+2.4
2a (compression knot)	1765.3	38×89.2	44.6	40.0	-4.6
2b (inverted, tension knot)	1765.3	38×89.2	44.6	50.7	+6.1
3a (center knot)	1663.7	38×89.2	44.6	41.8	-2.8
3b (inverted, center knot)	1663.7	38×89.2	44.6	35.6	-9.0
4a (tension knot)	1384.3	38×88.6	44.3	52.5	+8.2

[a]NA is above (+) or below (-) the half-distance.

below the centroid of the beam. In these circumstances the NA moves down to keep the internal tension and compression forces balanced. This is also in agreement with the findings of Betts et al. (2010) for Douglas fir.

38×89 mm beams

The NAs for the beams with larger dimensions do not behave quite as expected for clear specimens (Table 3). Each specimen was run once and then inverted, except for specimen 4a for experimental reasons (the beam was too short). In Table 3, 'a' denotes the specimen in its original orientation and 'b' the specimen inverted.

With the knot in compression (2a), the NA deviated 4.6 mm below the geometrical center of the beam (Table 3) and was located at 40 mm from tension face (bottom face), which is at about 45% of the depth of the beam, similar to the results published by Betts et al. (2010) (our reference paper for small clear beams). The beams with a knot in tension, beam 2b and beam 4a, had an average NA location at 50.7 mm (6.1 mm above centroid) and 52.5 mm (8.2 mm above centroid), respectively, from the tension face

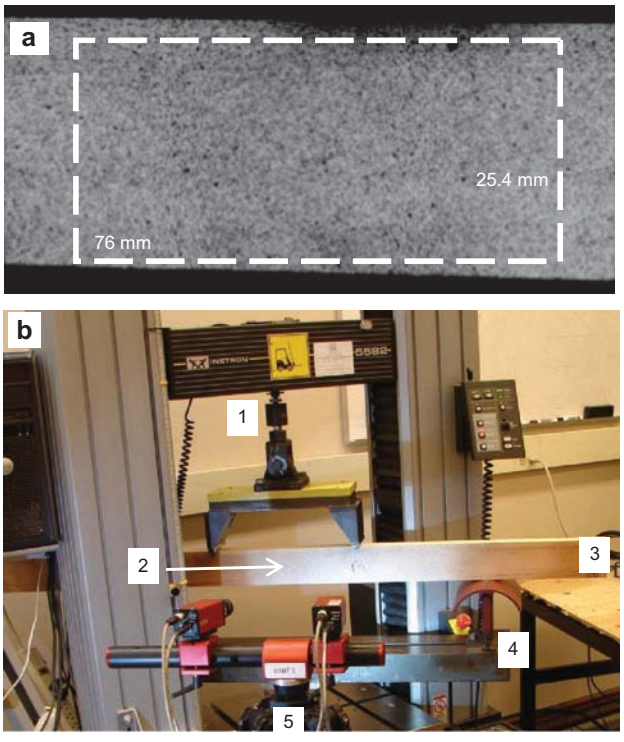

1 - Cross head; 2 - Speckle pattern;
3 - Specimen; 4 - End supports; 5 - DIC camera system

Figure 4 Sample, speckle pattern and area of interest for (a) digital image correlation (DIC) software and (b) DIC set-up.

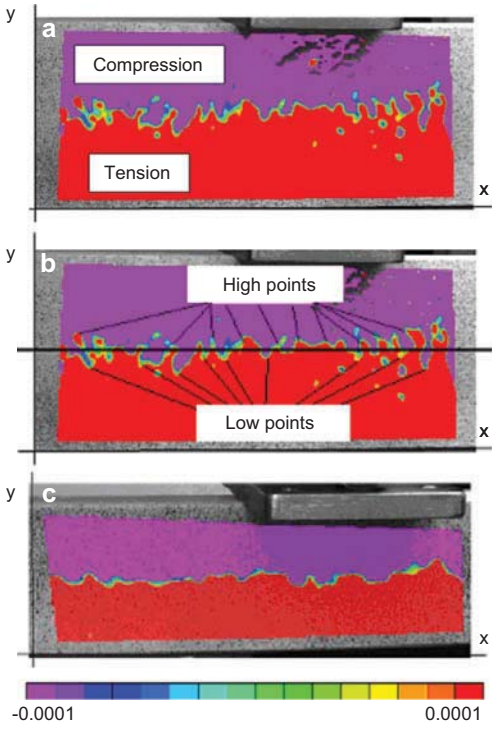

Figure 5 Contour plots using DIC and location of neutral axis. (a) Typical axial strain contour plot (ε_{xx}) at 75% peak load for Hem fir; (b) high and low point definition for determining neutral axis location at 75% peak load for Hem fir; (c) axial strain (ε_{xx}) plot for the steel beam.

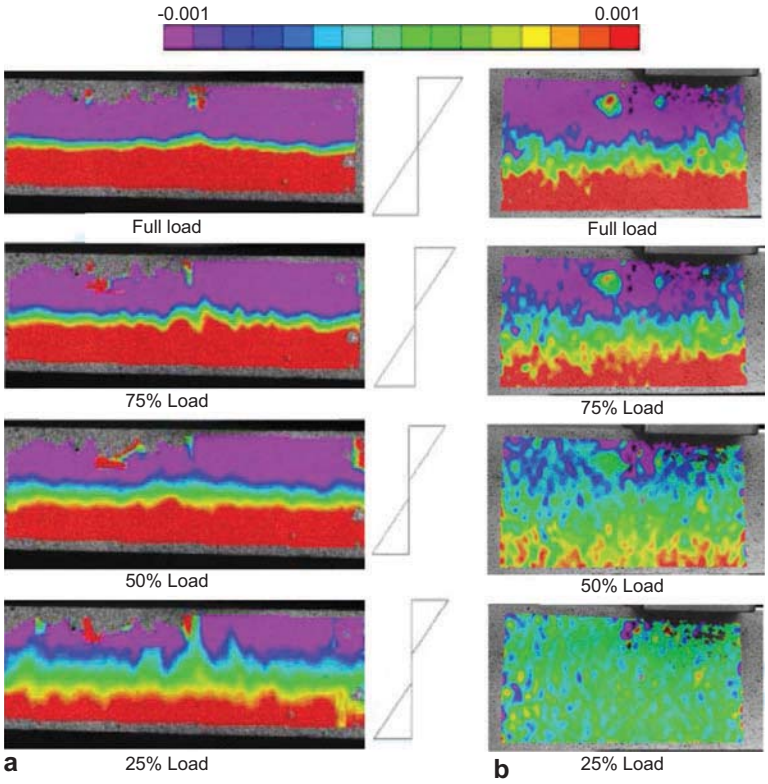

Figure 6 Axial strain (ε_{xx}) plots of Douglas fir beams showing the development of the neutral axis as a function of load. (a) For a 25×25 mm^2 clear beam and (b) for a 38×89 mm^2 beam with a compression knot.

(above the centroid) in agreement with the reference paper. In beams that contained a knot in the center, namely 3a and 3b, the NAs deviated 2.8 and 9.0 mm from the centroid, respectively. This corresponds to an average location for the NA at 44% of the tension face. In the reference paper, NA was reported to move up and around a knot. The clear specimens (1a and 1b) have a NA located at approximately 52% of the depth of beam measured from the tension face. Accordingly, the location is slightly higher than the centroid of the beam, deviating from the data of reference paper. This deviation can be easily explained: for the 25×25 mm beams in the reference paper, $MOE_{tensile}>MOE_{compr}$, so the NA is expected to be lower than the centroid. For larger wood beam sizes the opposite is true, i.e., $MOE_{tensile}<MOE_{compr}$, so the NA is located above the centroid. The specimen geometry (square 25×25 mm^2 small beams vs. 38×89 mm beams) should not, in theory, affect the bending behavior of the beams. However, this statement is true only if the material is isotropic and homogeneous, prerequisites which are not fulfilled by wood. The shifts reported above are mainly attributable to the stiffness of wood in tension and compression.

Steel beam

The NA for a homogeneous isotropic specimen should be located at the centroid of the beam and should be a clear straight line along the length of the beam (Gere and Timoshenko 1997), but this was not exactly the case in the present study. While the NA was much more clearly defined for the steel specimens than it was for the wooden beams, it was not perfectly straight as expected (Figure 5c). In addition, the NA location was 0.6 mm above the centroid, i.e., approximately 52% of the depth of the beam as measured from the tension face. The unexpected variations are possibly the result of imperfections in the metal or, more importantly, occurred because the steel specimen was not loaded to failure. Nevertheless, the steel specimen as an isotropic homogeneous material provides better means in comparison to wood (Figure 5c), thus its NA is more clearly defined than that of the wood beams (Figure 6a and b).

Development of the neutral axis (NA)

On the basis of all tests of the 25×25 mm^2 specimens, a trend was noticed for the NA development. The NA becomes more clearly defined as the bending progresses (Figure 6a). The contour plots in this Figure are software generated (see Experimental). As the data are imported step by step for various loading conditions, they are superimposed on the reference image. The NA development begins as a broad band and ultimately becomes a small, narrow band approximating a line. Accordingly, it is not a line at every loading phase, as it should theoretically be for isotropic materials. At one-quarter of the failure load, the neutral region is approximately 20%

Table 4 Maximum load, deviation of NA from centroid and comparison of theoretical and experimental results for strain at compression face for various small (25×25 mm^2) beams.

Specimen	Species	P_{max} (N)	NA from bottom face (mm)	Δ Deviation NA[a] (mm)	Strain ε		Δε (%)
					Calculated	Measured	
1	Douglas fir (clear)	2100	11.68	-1.02	0.01010	0.01040	3
2	Hem fir (compression knot)	1200	15.75	+3.05	0.00479	0.00785	40
3	Hem fir (tension knot)	2200	10.16	-2.54	0.00564	0.00200	182
4	Southern yellow pine (clear)	2700	11.68	-1.02	0.01150	0.04000	71
5	Hem fir (clear)	2200	10.16	-2.54	0.01210	0.03500	65
6	Alder (clear)	2700	11.18	-1.52	0.00858	0.02620	67
7	Oak (clear)	3700	11.43	-1.27	0.01250	0.01660	24

P_{max}, failure load; [a]NA is above (+) or below (-) the half-distance.

Table 5 Material and geometrical properties, testing parameters, strain (at compression/top face) and comparison for all dimensional lumber (38×89 mm^2) beams tested.

Specimen	P (N)	d (mm)	NA from bottom (mm)	Δ Deviation NA[a] (mm)	MOE (GPa)	ε (calc.)	ε (meas.)	Δε (%)
1	2700	2.42	46.2	+1.5	12.96	0.00060	0.00164	63
1 inverted	2871	2.60	47.1	+2.4	12.82	0.00064	0.00180	65
2	2221	2.58	40.0	-4.6	10.00	0.00070	0.00260	72
2 inverted	3179	3.25	50.7	+6.1	11.38	0.00073	0.00138	47
3	3638	3.11	41.8	-2.8	13.58	0.00086	0.00228	62
3 inverted	3965	3.59	35.6	-9.0	12.82	0.00110	0.00210	46
4	3471	3.49	52.5	+8.2	11.58	0.00075	0.00168	56
Metal	2983	4.31	24.4	+0.6	220.61	0.00060	0.00103	40

P (load) and d (deflection) were taken in the linear portion of the loading. [a]NA is above (+) or below (-) the half-distance; ε (calc.), calculated (theoretical) strain; ε (meas.), measured strain; MOE, modulus of elasticity.

of the cross section; at one-half of the failure load, the neutral region has decreased to approximately 13% of the cross section; at three-quarters of the failure load, the neutral region is approximately 10% of the cross section, and at the maximum load the broad neutral band shrinks to a neutral plane.

The same trend was also seen in the 38×89 mm^2 specimens (Figure 6b) but it is less pronounced. The neutral region is almost indistinguishable until the load reaches 50–75% of maximum (Figure 6b). In this loading region, the NA begins to be clear and the band narrows. Complete sets of images over the course of loading for all specimens can be found in Davis (2010).

Comparison of experimental and theoretical strains

The theoretical axial strain in each sample was calculated and compared to the experimental strain values (Tables 4 and 5). On average, the difference between the two values was somewhere between 25% and 70%. The deviations between the theoretical and measured strain oscillate in the range 3% and 182%. The high scattering of aberrations is a result of the ambiguous NA determination until the specimen approaches its maximum load. The equations used and all calculations (based on elastic beam theory) can be found in Davis (2010). The calculations assume a linear distribution of stresses. As a result, strain values were taken at approximately half of the maximum load to ensure that the beams were still in the elastic region. However, as stated above, the NA is broad band rather than a line, and in this case the beam theory used will not be accurate.

Conclusions

As would be expected, the NA for the 25×25 mm^2 clear specimens was slightly lower than the centroid of the beam. Knots in the tension or compression zones cause the NA to deviate away from the knots. Similar observations were made for the 38×89 mm^2 specimens with knots. The NA of the clear 38×89 mm specimens, however, was displaced above (and not below) the centroid. This is because $MOE_{tension}<MOE_{compr}$. More research is needed to confirm the presented preliminary results with a greater number of samples and specimens.

References

American Society for Testing and Materials (ASTM) (2009) D 143. Standard methods of testing small clear specimens of timber.

American Society for Testing and Materials (ASTM) (2009) D 198. Standard methods of static tests of lumber in structural sizes.

Bedford, A.M., Leichti, K.M. Mechanics of Materials. Prentice Hall, NJ, 2001.

Betts, S.C., Miller, T.H., Gupta, R. (2010) Location of the neutral axis in wood beams – a preliminary study. Wood Mater. Sci. Eng. 5:173–180.

Choi, D., Thorpe, J.L., Hanna, R.B. (1991) Image analysis to measure strain in wood and paper. Wood Sci. Tech. 25:251–262.

Correlated Solutions. Vic-3D User Manual. Correlated Solutions, Inc., Columbia, SC, 2005.

Davis, P.M. An Examination of the Neutral Axis of Wood Beams. University Honors College Thesis, Oregon State University 2010 (available from rakesh.gupta@oregonstate.edu).

Gere, J., Timoshenko, S. Mechanics of Materials (4th edition). PWS Publishing Co, 1997.

Green, D.W., Evans, J.W. Mechanical properties of visually graded lumber: Volume 1. A summary. U.S. Department of Agriculture, Forest Service, Forest Products Laboratory, Madison, WI, 1987.

Jeong, G.Y., Zink-Sharp, A., Hindman, D.P. (2010) Applying digital image correlation to wood strands: influence of loading rate and specimen thickness. Holzforschung 64:729–734.

Jernkvist, L.O., Thuvander, F. (2001) Experimental determination of stiffness variation across growth rings in *Picea abies*. Holzforschung 55:309–317.

Kang, H., Muszynski, L., Milota, M.R. (2011) Optical measurement of deformation in drying lumber. Drying Technology 29:127–134.

Kollen-Cumbie, R. Understanding the Orthotropic Behavior of Wood. Senior Project. Department of Wood Science and Engineering, Oregon State University, Corvallis, OR, 2008 (available from Rakesh Gupta: rakesh.gupta@oregonstate.edu).

Kollman, F.F.P., Cote Jr., W.A. Mechanics and rheology of wood (Chapter 7). In: Principles of Wood Science and Technology I: Solid Wood. Springer-Verlag, New York, 1968.

Kretschmann, D.E. Mechanical properties of wood (Chapter 5). In: Wood Handbook: Wood as an Engineering Material. General Technical Report FPL-GTR 190. U.S. Department of Agriculture, Forest Service, Forest Products Laboratory, Madison, WI, 2011.

Ljungdahl, J., Berglund, L.A., Burman, M. (2006) Transverse anisotropy of compressive failure in European oak – a digital speckle photography study. Holzforschung 60:190–195.

Lopes, S., Bernardo, L. (2004) Neutral axis depth versus flexural ductility in high-strength concrete beams. J. Struct. Engrg. 130: 452–459.

Modén, C.S., Berglund, L.A. (2008) Elastic deformation mechanisms of softwoods in radial tension – cell wall bending or stretching? Holzforschung 62:562–568.

Murata, K., Kanazawa, T. (2007) Determination of Young's modulus and shear modulus by means of deflection curves for wood beams obtained in static bending tests. Holzforschung 61:589–594.

Redler, H. (2006) Movement of Neutral Axis in Beams Subjected to Pure Bending. Submitted for a Reading and Conference Course class to Dr Rakesh Gupta at Oregon State University. Corvallis, OR (available from rakesh.gupta@oregonstate.edu).

Schniewind, A. Mechanical behavior and properties of wood. In: Wood: its Structure and Properties, Vol. 1. Eds. Wangaard, F.F., Clark, C. Heritage Memorial Series on Wood. Pennsylvania State University, University Park, PA, 1981.

Sebera, V., Muszyński, L. (2011) Determination of local material properties of OSB sample by coupling advanced imaging techniques and morphology-based FEM simulation. Holzforschung 65:811–818.

Serrano, E., Enquist, B. (2005) Contact-free measurement and nonlinear finite element analyses of strain distribution along wood adhesive bonds. Holzforschung 59:641–646.

Sinha, A., Gupta, R. (2009) Strain distribution in OSB and GWB in wood-frame shear walls. J. Struct. Engrg. 135:666–675.

Sutton, M.A., Wolters, W.J., Peters, W.H., Rawson, W.F., McNeill, S.R. (1983) Determination of displacements using an improved digital image correlation method. Image Vis. Comput. 1:133–139.

Received July 29, 2011. Accepted October 24, 2011.
Previously published online November 25, 2011.